Szeliga *et al. Earth, Planets and Space (2022) 74:193*
https://doi.org/10.1186/s40623-022-01748-6

Earth, Planets and Space

FULL PAPER

Open Access

Historical tsunami observability for Izu–Bonin–Mariana sources

Walter Szeliga[1*], Rachelle Reisinger[2] and Breanyn MacInnes[1]

Abstract

The Izu–Bonin–Mariana Subduction System (IBM) is one of the longest subduction zones in the world with no instrumental history of shallow focus, great earthquakes (Mw > 8). Over the last 50 years, researchers have speculated on the reason for the absence of large magnitude, shallow seismicity on this plate interface, exploring factors from plate age to convergence rate. We approach the question from a different point of view: what if the IBM has hosted great earthquakes and no documentable evidence was left? To address the question of observability, we model expected tsunami wave heights from nine great earthquake scenarios on the IBM at selected locations around the Pacific Basin with an emphasis on locations having the possibility for a long, written record. Many circum-Pacific locations have extensive written records of tsunami run-up with some locations in Japan noting tsunami back to 684 CE. We find that most IBM source models should theoretically be observable at historically inhabited locations in the Pacific Basin. Surprisingly, however, some IBM source models for earthquakes with magnitudes as high as Mw 8.7 produce tsunami wave heights that would be essentially unobservable at most historically populated Pacific Basin locations. These scenarios aim to provide a constraint on the upper bound for earthquake magnitudes in the IBM over at least the past 400 years.

Keywords: Tsunami observability, Izu–Bonin–Mariana, Numerical modeling

*Correspondence: Walter.Szeliga@cwu.edu

[1] Central Washington University, Ellensburg, WA, USA
Full list of author information is available at the end of the article

Graphical Abstract

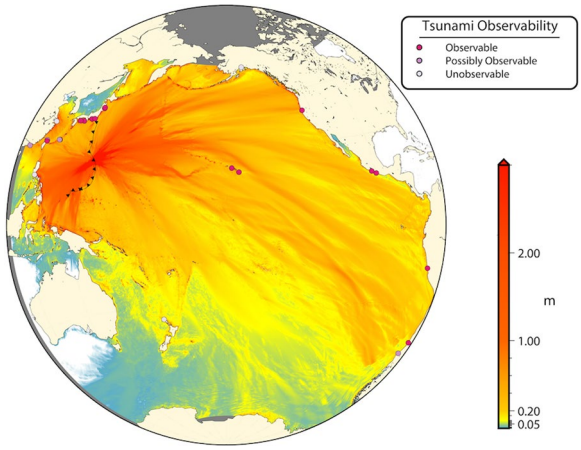

Introduction

Our understanding of tsunamis has grown over the past century following the instrumental observation of multiple, large, ocean-crossing tsunamis triggered by subduction zone earthquakes. Due to the destructive potential from violent shaking and the subsequent tsunami from these earthquakes, many studies have been conducted in the past 50 years on subduction zones globally and their ability to produce large earthquakes, as not all subduction zones are thought to be capable (Singh et al. 1981; Goldfinger et al. 1992; Johnson and Satake 1999; Barnes et al. 2002; Satake and Atwater 2007). Although initially proposed as an explanation for the presence or absence of back-arc spreading, the classification of subduction zones into Mariana-type and Chilean-type appeared to provide further explanatory power with regard to the mode of seismic strain release at each boundary (Uyeda and Kanamori 1979). Subsequent studies continued to develop the Chilean–Mariana subduction style classification paradigm (Ruff and Kanamori 1980; Kanamori 1986; Ruff 1989; Stern 2002; Stern et al. 2003). In particular, regression analysis of slab age, convergence rate, and maximum earthquake magnitude all seemed to confirm this classification scheme (Ruff and Kanamori 1980). One of the outcomes of this regression analysis was the prediction that some subduction zones, including northern Japan, Sumatra, and Cascadia, had a maximum earthquake magnitude less than Mw 9 (Heaton and Kanamori 1984; Kanamori 1986). In the case of the Mariana and Izu–Bonin subduction systems, the predicted maximum earthquake magnitude according to the Chilean–Mariana subduction style classification paradigm is even smaller, possibly less than Mw 7.6 (Kanamori 1986).

The realization that the Cascadia subduction zone had experienced a great earthquake in 1700 (Satake et al. 1996) along with the subsequent great earthquakes in Sumatra (2004) and northern Japan (2011) provided direct refutations of the predictions from this classification scheme. Following these earthquakes, numerous researchers began to question the assumption that some subduction zones cannot host great earthquakes (McCaffrey 2008; Stein and Okal 2011; Kagan and Jackson 2013; Rong et al. 2014). Under this new wave of thinking that all subduction zones can host large tsunamigenic earthquakes, the physical dimensions of the subduction zone itself are thought to be the best predictors of maximum earthquake magnitude. For the Izu–Bonin–Mariana subduction system, this approach yields a value of Mw 9.2 for the Izu segment and Mw 9.5 for the Mariana segment (McCaffrey 2008). McCaffrey (2008) also provides a prediction of recurrence interval with estimates of 723 years for the Izu segment and 893 years for the Mariana segment.

Given the limited time span of the instrumental seismic record, extending our knowledge of great earthquakes further into the past must rely on historical documentation of seismic events, mostly in the form of felt reports of shaking and inundation from tsunami. This approach

has yielded immense knowledge in regions where the written record is long, such as Japan (Ishibashi 2004; Matsu'ura 2017). However, for great earthquakes in remote or sparsely populated regions, the historical record is likely incomplete. This study addresses the possibility of identifying historical earthquakes in the Izu–Bonin–Mariana region from the standpoint of tsunami visibility in the far-field: if a large earthquake occurred in the Izu–Bonin–Mariana region, which areas of the Pacific Basin would be most likely to have recorded the effects of the ensuing tsunami? We then interrogate the historical record for some of these locations looking for signs of recorded tsunami.

Background

The instrumental earthquake history of the IBM is limited (< 130 years) with the largest recorded earthquake being a Mw 7.8 on August 8, 1993, with a focal depth of nearly 60 km (Fig. 1) (US Geological Survey 2017; Harada and Ishibashi 2008). This earthquake, along with earthquakes of Mw 7.0 and 7.1 in 2001 and 2002 near Guam have been the subject of interest as being some of the largest magnitude shallow forearc seismicity in the Mariana region (Tanioka et al. 1995; Campos et al. 1996; Harada and Ishibashi 2008). Farther north, along the Izu–Bonin segment of the IBM, the largest instrumentally recorded earthquake was the December 21, 2010 Mw 7.4 Bonin Islands earthquake near Hahajima, Japan (US Geological Survey 2017). Although this earthquake was a shallow-focus outer-rise normal faulting event in the Pacific Plate, and not on the subduction interface, it nonetheless caused a 7–13 cm tsunami along the south coast of Honshu (National Tsunami Warning Center).

The tsunami history for the Izu–Bonin and Mariana Islands, including the Caroline Islands and Guam extends back to at least 1606 with the description of a tsunami accompanying a volcanic eruption on Hachijō-jima in the northern Izu Islands (Fig. 1) (Soloviev and Go 1984a, b). The earliest tsunami attributable to an earthquake from the Izu–Bonin–Mariana arc is likely the earthquake and tsunami of January 1826, whose shaking and tsunami effects were felt strongly on Chichijima in the Bonin Islands (Fig. 1) (Soloviev and Go 1984a, b). A larger and more destructive earthquake, with a long-lived aftershock sequence and tsunami, occurred near Guam in January of 1849 (Fig. 1). The mainshock of this earthquake razed all of the masonry structures on the island and caused a tsunami that may have inundated Guam for a distance of 500 m and may also have been recorded on the atoll of Satawal in the Caroline Islands over 700 km SSE of Guam (Fig. 1) (Soloviev and Go 1984a, b; Lander et al. 2002). Additional earthquakes and tsunami were recorded in the Bonin Islands on the island of Chichijima in the fall of

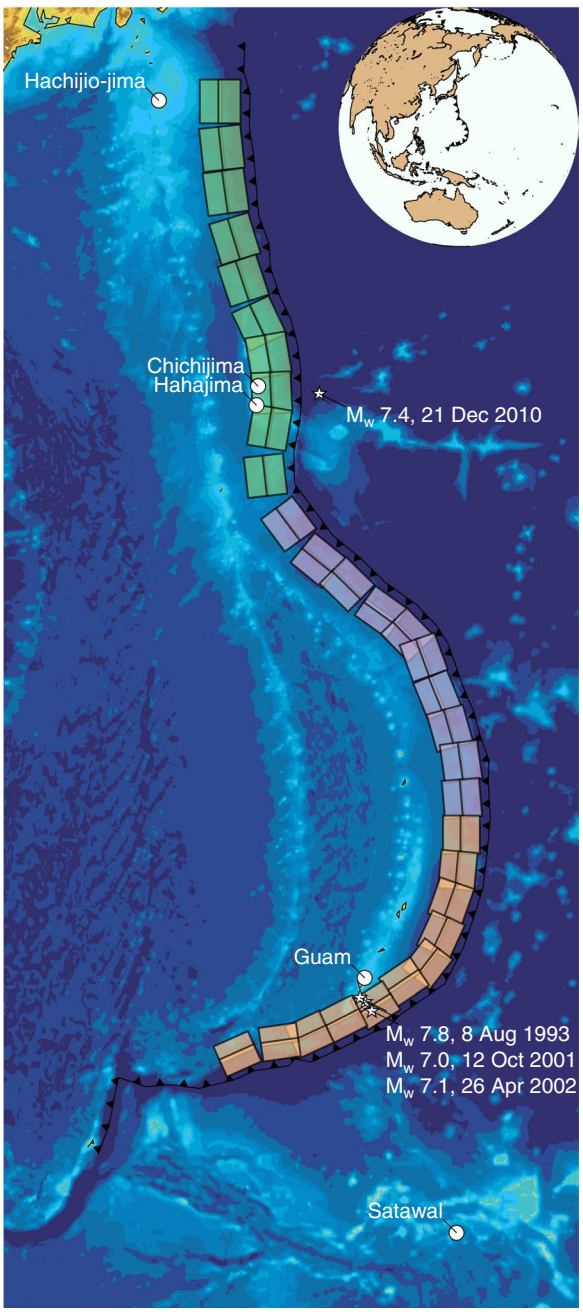

Fig. 1 Location of the Izu–Bonin–Mariana subduction system. Stars represent the four largest, shallow focus, instrumentally located earthquakes in the subduction system. Circles represent locations mentioned in this manuscript. Colored rectangles denote faults from the NOAA SIFT fault model database. The colors represent the fault segments used in this paper: the green segment is the Izu–Bonin segment, the purple segment is the north Mariana, and the orange is the south Mariana segment

1872 (supposedly also recorded in the Hawaiian Islands, although this is less certain. See Cox and Lander (1994) and references therein for further discussion) (Cholmondeley 1915; Soloviev and Go 1984a, b), and 1892 (felt in Guam) (Soloviev and Go 1984a, b). Subsequent tsunamis in the region appear to have been volcanic or meteorologic in origin (Soloviev and Go 1984a, b). More recently, the instrumentally recorded Mw 7.8 earthquake of August 8, 1993 produced a tsunami with wave heights of around 20 cm on a tide gauge at Mera, Japan, on the southern end of the Bōsō Peninsula (Tanioka et al. 1995). Local effects from the August 8, 1993 tsunami were more pronounced on the island of Guam (Sigrist 1995).

Modeling

To assess far-field tsunami visibility, we produce generalized models of tsunami generated by large, shallow subduction zone earthquakes from the IBM. Using the IBM subduction zone fault geometry from the National Oceanic and Atmospheric Administration (NOAA) Short-term Inundation Forecasting for Tsunami (SIFT) fault model database (Gica et al. 2008), we model earthquakes with magnitudes from Mw 8.7 to Mw 9.3 with smoothly varying slip centered at different locations along the IBM. We then use the resulting surface deformation as a starting model for GeoClaw V5.7 to model the resulting tsunami waveform across the Pacific Basin. Time series of water surface height are then calculated at select, shallow water locations around the Pacific Basin as a proxy for tsunami arrival height.

In order to characterize the general tsunami behavior of earthquakes in the IBM, we begin by dividing the IBM into fault segments. Since the majority of a tsunami's energy is directed perpendicular to the strike of its causal earthquake (Ben-Menahem and Rosenmen 1972), we partition the IBM into segments based on the overall strike of the subduction system. This partitioning allows us to study the overarching directivity patterns of IBM-generated tsunami but is not intended to imply the existence of barriers to slip or other rupture kinematic behavior. Ruptures that span the fault segments highlighted here should produce tsunami with directivity patterns that display characteristics of each segment in a manner similar to what is seen with the NOAA SIFT approach (Gica et al. 2008). Following the large-scale strike of the IBM, we partition the subduction zone into three segments (Fig. 1): From north to south, an Izu–Bonin segment (Fig. 1, green fault); a northern Mariana segment (Fig. 1, purple fault), and a southern Mariana segment (Fig. 1, orange fault).

For each of these fault segments, we then model three slip distributions with magnitudes Mw 8.7, 9.0 and 9.3, each with a smooth Gaussian-like slip profile along strike (Additional file 1: Table S1 and Additional file 2: Figure S1). For each dislocation source and for each fault segment, we simulate the propagation of a tsunami to each circum-Pacific location listed in Table 1. In choosing circum-Pacific locations for forward modeling, we endeavored to select locations with known written records of past tsunami. Based on these criteria, 23 locations were selected (Fig. 2, Table 1). Tsunami simulations were then performed using GeoClaw 5.7 (Clawpack Development Team 2020) with grid refinement guided by the adjoint method (Davis and LaVeque 2016). Bathymetric grid refinement cell sizes ranged from 1° to 30 arcsec using bathymetry from GEBCO 2019 (GEBCO Compilation Group 2019). Example tsunami waveforms are shown in Additional file 3: Figures S2 and Additional file 4: Figure S3.

Since GeoClaw solves the depth-averaged shallow water equations, they provide the best approximation of water height when the wavelength is long relative to the depth of the water. In order to capture wave heights in shallow water while retaining the full waveform, we attempted to keep our gauge locations in water depths shallower than 20 m. Additionally, GeoClaw does not estimate tsunami dispersion. For our tsunami scenarios, the rupture widths are approximately 90 km and lie in water that is, on average 4000 m deep. Using these values in Eq. (1) of Shuto (1991), we expect tsunami dispersion to be negligible to distances of at least 4000 km. Beyond this distance, preliminary modeling using JAGURS (Baba et al. 2015) suggests that dispersion may result in a limited reduction in amplitude in dispersed wave trains at the furthest distances from the tsunami source (Additional file 5: Figure S4). Similar results can be seen for trans-oceanic paths for the 2011 Tohoku tsunami (Baba et al. 2017). Thus, maximum wave height model results using output from GeoClaw will represent a worst-case scenario at the furthest gauge locations.

Finally, in order to assess the far-field impact of each tsunami scenario, we have developed a basic tsunami observability index based on the relative amplitude of the largest wave with respect to the local tidal variation. Since we are interested in historical observability, the mean range of tides for a location, defined as the difference in height between the mean high water and the mean low water (Gill and Schultz 2001), provides a reasonable benchmark that an observer familiar with the typical tidal variations at a location might use in recognizing an incoming tsunami. Using tidal datum information provided by the GLOSS Network (Caldwell et al. 2015), the mean range of tides was identified for each location and is listed in Table 1.

Our tsunami observability index consists of three observability categories, *Unobservable*, *Possibly*

Table 1 Water height sampling locations, model water depth, earliest tsunami record, and tidal range for locations modeled in this manuscript

Gauge no.	Name	Location	Tsunami model water depth (m)	Earliest tsunami record	Tidal range (mean range of tide MN [m])	Tidal range source
1	Keelung, Taiwan	25.157212°, 121.753822°	2.9	1754 (Soloviev and Go 1984a, b; NCEI/WDS)	0.49	https://uhslc.soest.hawaii.edu/stations/?stn=341#datums
2	Toucheng, Taiwan	24.855488°, 121.835878°	8.2	1754 (Soloviev and Go 1984a, b; NCEI/WDS)	0.49	Interpolated from Keelung
3	Ginowan, Okinawa	26.262317°, 127.807741°	4.8	1687 (NCEI/WDS), 1768 (Soloviev and Go 1984a, b)	1.23	Interpolated from Naha
4	Naha, Okinawa	26.212919°, 127.643609°	4.3	1687 (NCEI/WDS), 1768 (Soloviev and Go 1984a, b)	1.23	https://uhslc.soest.hawaii.edu/stations/?stn=355#datums
5	Tanabe, Japan	33.718603°, 135.361647°	10.4	869 (at Iwashiro, NCEI/WDS), 1700 (NCEI/WDS)	0.99	https://uhslc.soest.hawaii.edu/stations/?stn=353#datums
6	Kochi, Japan	33.502806°, 133.576283°	5.5	684 in Tosa (Soloviev and Go 1984a, b; NCEI/WDS), 1707 specifically in Kochi, (NCEI/WDS)	0.99	Interpolated from Tanabe
7	Miho, Japan	34.997555°, 138.528487°	17	1096 (at Shizuoka, NCEI/WDS), 1700 (NCEI/WDS)	0.80	Interpolated from Futtsu
8	Otsuchi, Japan	39.342525°, 141.947532°	6.2	1088 (along Sanriku Coast, NCEI/WDS), 1616 (NCEI/WDS)	0.71	Interpolated from Kuwagasaki
9	Futtsu, Japan	35.291139°, 139.842699°	0.2	818 (in Boso Peninsula region, NCEI/WDS, Soloviev and Go 1984a, b), 1923 (earliest where Futsu was specifically named, NCEI/WDS)	0.80	https://uhslc.soest.hawaii.edu/stations/?stn=352#datums
10	Kuwagasaki, Japan	39.659536°, 141.978583°	1.7	869 (in Rikuchu, NCEI/WDS), 1677 (NCEI/WDS)	0.71	https://uhslc.soest.hawaii.edu/stations/?stn=351#datums
11	Shanghai, China	31.083193°, 122.052908°	5.1	1498 (NCEI/WDS, Zhao et al. 2017), 1509 (Soloviev and Go 1984a, b) Possibly 1496, July 9 (Liu et al. 2007)	2.69	OTPS Calculation
12	Hong Kong Island, Hong Kong	22.210770°, 114.266769°	7.4	1767? (in Macau, NCEI/WDS, Lau et al 2010)	0.94	https://uhslc.soest.hawaii.edu/stations/?stn=329#datums
15	Manila, Philippines	14.561631°, 120.964339°	5.1	1645 (Soloviev and Go 1984a, b)	0.69	https://uhslc.soest.hawaii.edu/stations/?stn=370#datums
16	Honolulu, United States	21.296236°, − 157.871507°	4.4	1812 (or sometime between 1500–1600) (Pararas-Carayannis 1977; Lander and Lockridge 1989)	0.39	https://tidesandcurrents.noaa.gov/stationhome.html?id=1612340
17	Hilo, United States	19.735757°, − 155.078875°	7	1819 (or 1812 or sometime between 1500–1600, Lander and Lockridge 1989)	0.51	https://tidesandcurrents.noaa.gov/stationhome.html?id=1617760
18	Anchorage, United States	61.207397°, − 150.138107°	21.5		7.98	https://tidesandcurrents.noaa.gov/stationhome.html?id=9455920

Table 1 (continued)

Gauge no.	Name	Location	Tsunami model water depth (m)	Earliest tsunami record	Tidal range (mean range of tide MN [m])	Tidal range source
19	Henderson Bay, NZ	−34.694446°, 173.064344°	4.1	1835 (GNS Science 2020)	2.87	Spring range for Auckland from https://www.linz.govt.nz/sea/tides/tide-predictions/standard-port-tidal-levels
20	Crescent City, United States	41.746751°, −124.211337°	5.8	1938 (NCEI/WDS; Lander et al 1993)	1.52	https://tidesandcurrents.noaa.gov/stationhome.html?id=9419750
21	Acapulco, Mexico	16.847925°, −99.878825°	10.1	1732 (NCEI/WDS; Sanchez and Farreras 1993; Soloviev and Go 1984b)	0.42	https://uhslc.soest.hawaii.edu/stations/?stn=316#datums
22	Ixtapa, Mexico	17.655679°, −101.642393°	10.5	1985 (NCEI/WDS)	0.42	Interpolated from Acapulco
24	Lima, Peru	−12.096937°, −77.106596°	8.8	1586 (NCEI/WDS; Beringhausen 1962)	0.45	https://uhslc.soest.hawaii.edu/stations/?stn=093#datums
25	Concepcion, Chile	−36.860250°, −73.164318°	18.6	1562 (NCEI/WDS; Soloviev and Go 1984b; Lockridge 1985)	0.95	OTPS Calculation
26	Valparaiso, Chile	−33.039464°, −71.613004°	23	1657(NCEI/WDS)		

Modeling locations are referred to as model gauges. Gauge number locations are shown in Fig. 2. The water depth at each gauge is a function of the adaptive grid algorithm and the input grid size of the bathymetry

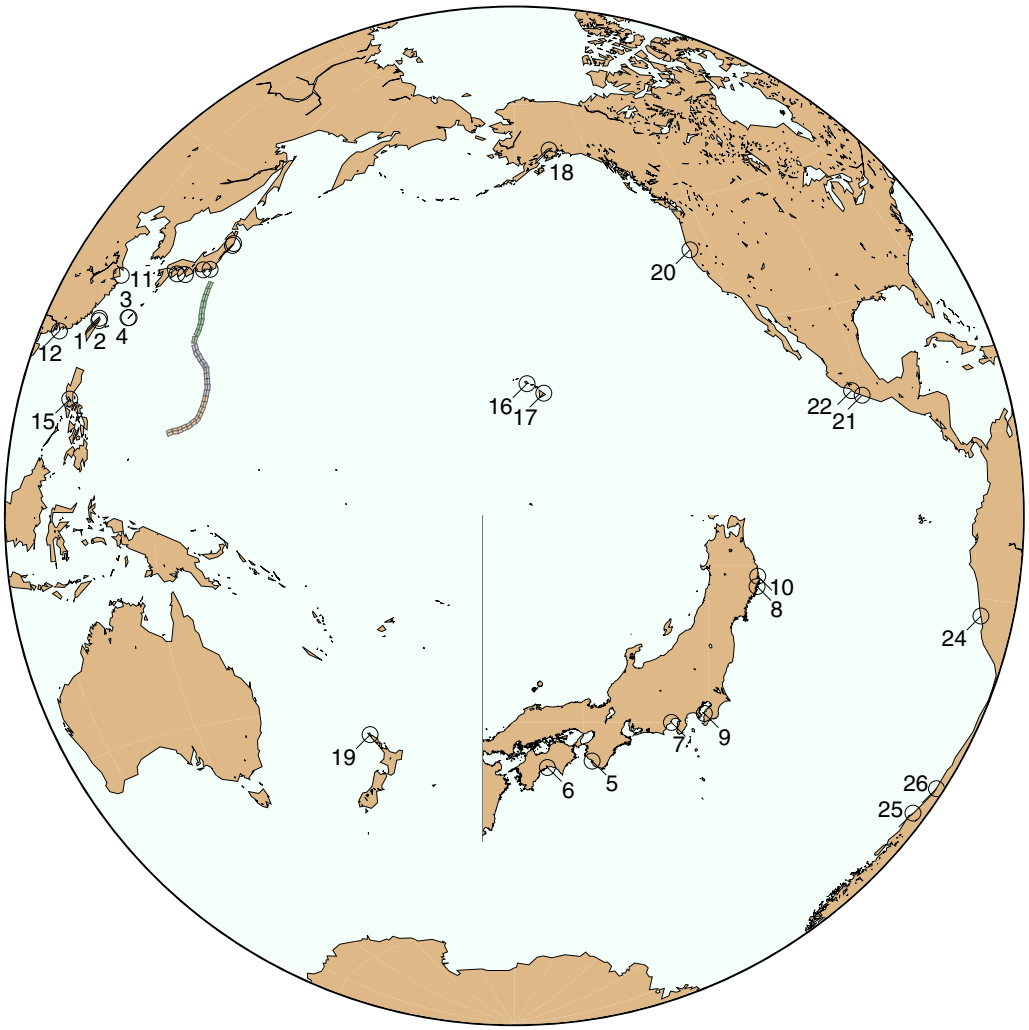

Fig. 2 Gauge locations from Table 1. Inset map shows the location of gauges along the east coast of Japan. Rectangles represent the location of the Izu–Bonin–Mariana fault segments shown in Fig. 1

Observable, and *Likely Observable*. In order to identify reasonable boundaries for these categories, we examined records of non-instrumental tsunami observations in the NCEI/WDS tsunami database (National Geophysical Data Center 2022). The NCEI/WDS tsunami database lists 558 non-instrumental, tsunami observations (defined in the database as "eyewitness measurement" and source validity "Definite Tsunami") with amplitudes less than 1 m. While there are some records of eyewitness measurements of maximum water heights as small as 0.1 m (~4 in., e.g., observations of the 1923 Kanto, Japan earthquake in Wellington, New Zealand; Soloviev and Go 1984a, b; de Lange and Healy 1986; National Geophysical Data Center 2022), most of the entries for water heights this small directly refer to marigraph measurements rather than visual observation of the ocean surface. The smallest reliable eyewitness observations of a tsunami without the aid of a marigraph or tide gauge are likely the 1906 Ecuador earthquake as observed in Gisborne, NZ (0.25 m; 15% of the tidal range; GNS Science 2020; National Geophysical Data Center 2022), the 1854 Nankaido earthquake as observed from Shimoji, Japan (0.3 m; 30% of the tidal range; Soloviev and Go 1984a, b; National Geophysical Data Center 2022), and the 1867 Virgin Island earthquake as observed from La Baye (Grenville), St Andrew Parish, Grenada (0.3 m; where the tsunami was described as "the wave was just discernable"; 89% of the tidal range; O'Loughlin and Lander 2003; National Geophysical Data Center 2022). Thus, we propose a cut-off between the categories of *Unobservable* and *Possibly Observable* for water heights at 30% of the tidal range at a given location. Similarly, we propose that any observation that is greater than 100% of the local tidal range as *Likely Observable*.

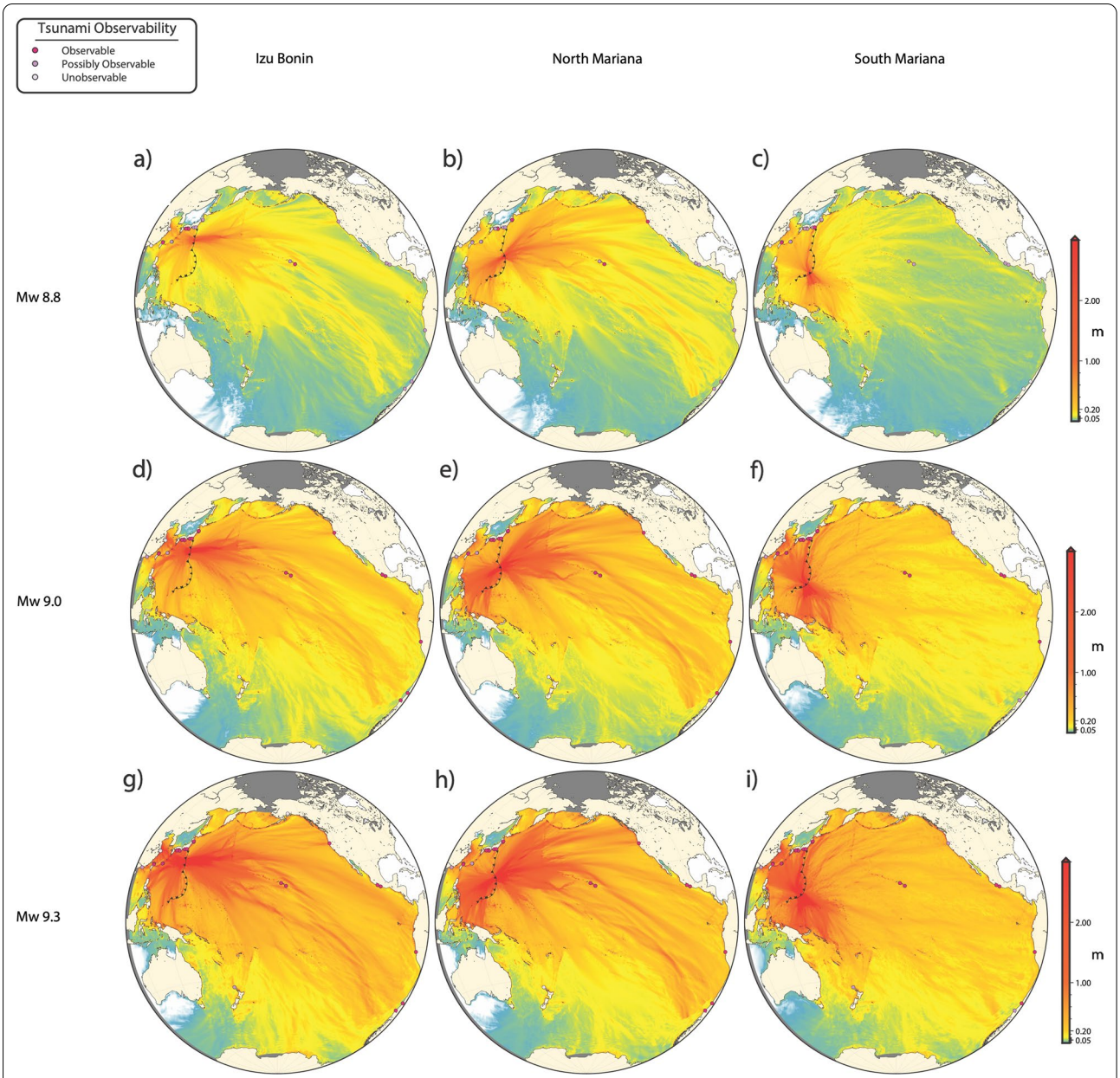

Fig. 3 Maximum wave height and tsunami observability for earthquake scenarios in the Izu–Bonin–Mariana subduction system. Figures a-c show maximum wave heights for earthquakes of magnitude M_w 8.7 for the Izu–Bonin (a), North Mariana (b), and South Mariana (c) sources. Figures d-f show maximum wave heights for earthquakes of magnitude M_w 9.0 for the Izu–Bonin (d), North Mariana (e), and South Mariana (f) sources. Figures g-l show maximum tsunami wave heights for magnitude M_w 9.3 earthquakes for the Izu–Bonin (g), North Mariana (h), and South Mariana (i). Filled circles represent tsunami visibility with the darkest purple indicating maximum wave heights in excess of the local tidal range, medium purple representing maximum wave heights larger than 30% of the local tidal range, and the lightest purple indicating maximum wave heights less than 30% of the local tidal range. All plots use the same color scale for maximum wave height

Hypothetical observability of large Mariana tsunamis

Figure 3 shows the results of the modeling for each of the faulting scenarios. Earthquakes with magnitude Mw 9.3 produce tsunamis with wave heights in excess of the local tidal range at nearly all Pacific Basin locations and therefore fall into the category of *Likely Observable*. For Mw 9.0 earthquake scenarios, nearly all locations in Japan show wave heights in excess of twice the tidal range (Table 1, Fig. 3), suggesting that observers in Japan would have had the opportunity to observe tsunami from these earthquakes. Similarly, for observers on the west coast of

the America's, nearly all locations show maximum wave heights in excess of the local tidal range for sources in the Izu–Bonin and North Mariana segments, while sources from the South Mariana exceed the local tidal range only at lower latitudes. For Mw 8.7 earthquake scenarios, Izu–Bonin sources direct tsunami wave energy towards locations near Shikoku, where maximum wave heights rise well above the local tidal range, however locations elsewhere in Japan experience maximum wave heights below the local tidal range (Table 1). Along the west coast of the Americas, Izu–Bonin sources also produce smaller wave heights, with most locations at around 50% of the tidal range. In contrast, Northern Mariana sources produce large wave heights at Crescent City, CA, while wave heights in Japan exceed the tidal range at Tanabe (Wakayama Prefecture) and along the northeast coast of Honshu. For Northern Mariana sources wave heights elsewhere in Japan are less than the tidal range. Finally, Southern Mariana sources produce mostly *Possibly Observable* wave heights in Japan with a localized large maximum wave height in Tokyo Bay (Futtsu, Chiba Prefecture) likely due to topographic wave guiding by bathymetric structures in the Izu–Bonin back-arc (Satake and Kanamori 1991).

For many locations, the Mw 8.7 sources produce maximum wave heights of about half of the local mean range of tides. At this amplitude, it is uncertain whether tsunami would be consistently observed at all hours of the day, under all tidal stages, or in all weather conditions.

Observability compared to the historical record

Table 1 lists our present knowledge of the earliest written record of tsunami for each location we have considered. The presence of written records at these times suggests that records of notable natural phenomena were kept in each region and that these records exist to the present day. In seeking out the locations with the longest written records of such events, we are attempting to place bounds on the length of time of quiescence of the Izu–Bonin–Mariana system. We do note that, although many locations have written records of tsunami dating back hundreds of years, this does not indicate that these written records are complete. The completeness of any written sources depends strongly on both preservation and access, including physical and linguistic access (e.g., Ambraseys and Melville 1982; Martin et al. 2020). The transmission and survival of historical tsunami data depends on historical and geographical circumstances which are not consistent throughout a region or across time. For example, examination of Fig. 3e–i suggests that the north coast of New Guinea would experience wave heights in excess of 2 m for both North and South Mariana sources larger than Mw 9.0 and possibly in excess of 5 m for Mw 9.3 sources. However, these locations were not modeled with gauges due to the presumed lack of a written historical record for northern New Guinea prior to the instrumental period (Lutton 1991; Nagle 2002). Similarly, for Northern Mariana tsunami sources, locations along the east coast of the Philippines would experience wave heights in excess of 5 m. However, in contrast to New Guinea, the Philippines possess a large, though untapped archive of Spanish documents, although pre-Spanish written history records appear to be non-existent (Punzalan 2006). Finally, many cultures in the Pacific Basin retain legends and folklore surrounding earthquakes and tsunami; the full appreciation of which is only starting to be realized (e.g., Ludwin et al. 2007). Given all these caveats, we note that the present study is not intended to suggest that the lack of a tsunami record is evidence that no tsunami occurred (an argument from ignorance), rather, our focus is on identifying locations that should prove to be fruitful areas for future historical research.

The earliest written records in the Pacific Basin we considered pertain to the earthquake and tsunami of 684, which occurred in the Kochi prefecture of Japan (National Geophysical Data Center 2022). Tsunami from this earthquake was recorded at Tosa, Japan, which is represented by our gauge location in Urado Bay near present day Kochi (Table 1, Gauge 6). Records in the Kochi Prefecture subsequently show tsunami in 1605 and then in 1707. To the east, in Wakayama Prefecture, Japan, records for a tsunami in 869 exist at Iwashiro, near our Tanabe Gauge (Table 1, Gauge 5). The 869 tsunami at Iwashiro was followed by a tsunami in 1099. The number of records increases starting around 1403 indicating an improvement in the completeness of the observations for this location. Further east in Shizuoka Prefecture, Japan, the earliest record is of a tsunami in 1096 with subsequent records increasing in frequency beginning in 1498. Tsunami in Shizuoka Prefecture is represented by our Miho gauge (Table 1, Gauge 7). Near the entrance to Tokyo Bay, in Chiba Prefecture, Japan, the earliest recorded tsunami is from 818. However, consistent records of tsunami do not begin at that location until 1602. Northward, along the Pacific Coast in Iwate Prefecture, Japan, records of the 869 tsunami exist, followed by tsunami in 1088 and 1257. In this region along the northwest coast of Honshu, the record of tsunami appears to be more complete beginning around 1611. Figure 4 summarizes the historical record of tsunami at our Japanese gauge locations.

Along the east coast of mainland China, the earliest recorded tsunami in Shanghai is in 1498 (Zhao et al. 2017; National Geophysical Data Center 2022). Followed by tsunami in 1668, 1854, 1867, and 1983 (Zhao et al. 2017; National Geophysical Data Center 2022).

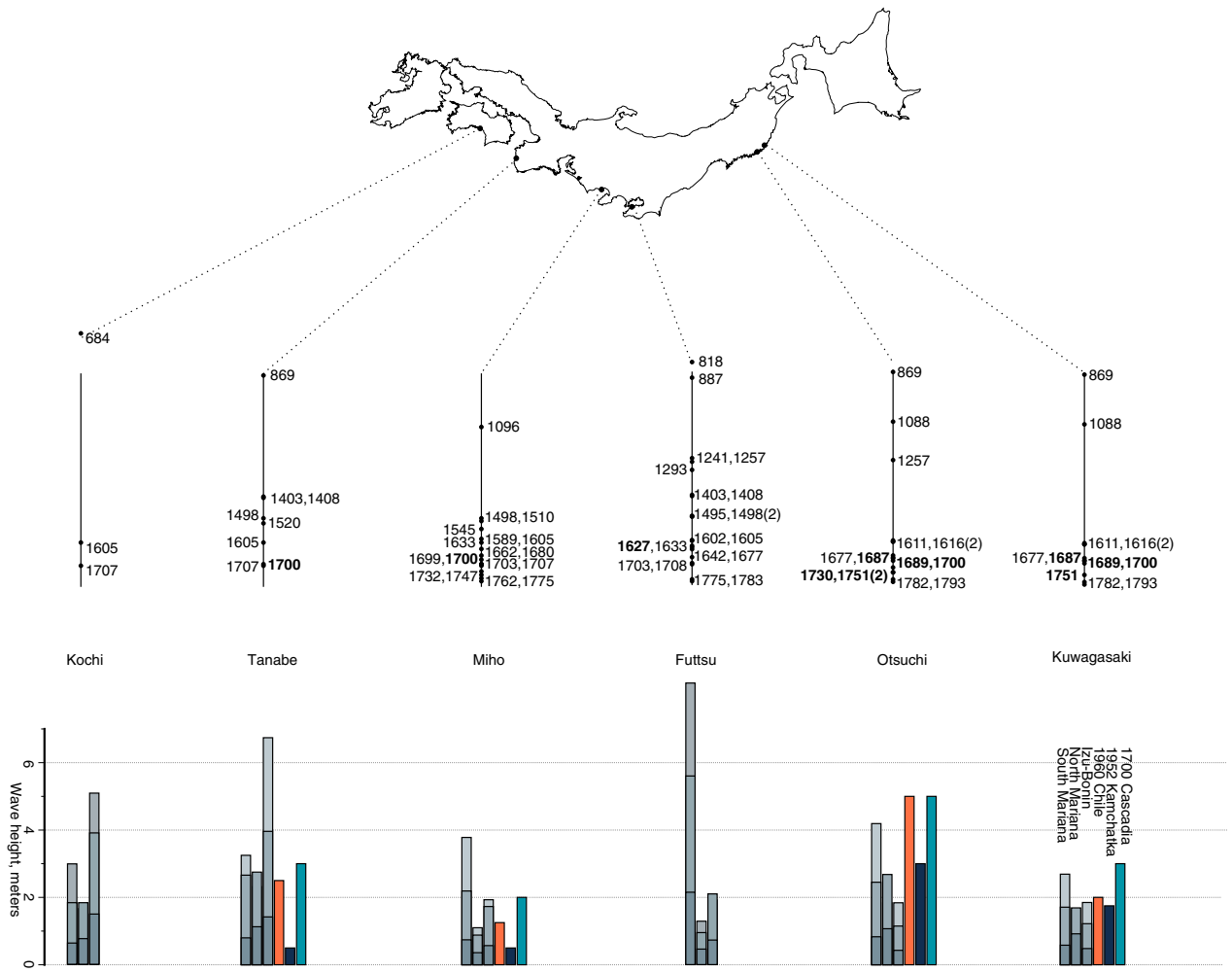

Fig. 4 Historical record of tsunami prior to 1800 with wave heights for select Japanese locations. Vertical lines denote times of written records of tsunami at each location. Bold values indicate orphan tsunami (i.e., tsunami without local shaking). All timelines end at the year 1800 and are to scale. Wave heights at select locations for tsunami sources in the Izu–Bonin, North Mariana, and South Mariana are from this work, while wave heights from the 1700 Cascadia tsunami (green), 1952 Kamchatka tsunami (dark blue), 1960 Chile tsunami (orange) are from Atwater et al., [2005]. Izu–Bonin, North Mariana, and South Mariana wave heights are stacked, showing tsunami wave heights from M_w 8.7 earthquakes in dark gray, those from M_w 9.0 earthquakes in gray, and those from M_w 9.3 earthquakes in light gray

Along the west coast of the Americas, the earliest recorded tsunami is the 1562 tsunami observed at Concepción, Chile. Tsunamis in the BioBío region around Concepción are then regularly recorded up to the present day at a rate of 2.5 events per century. Further north along the South American coast, the earliest recorded tsunami in Lima, Peru is in 1586. Similar to records at Concepción, eyewitness reports of tsunami at Lima continue to the present day, averaging 2.5 events per century.

The earliest written tsunami records for other locations around the Pacific Basin are more recent, with records in Manila, Philippines, in 1645; Acapulco, Mexico, in 1732; Keelung, Taiwan, in 1754; Honolulu, Hawaii, in 1812; and Auckland, New Zealand (Henderson Bay), in 1835 (Table 1).

By taking into consideration the length and completeness of historical tsunami observations along with the predicted wave heights, we come to the following conclusions. For Izu–Bonin tsunami sources, the most reliable locations for observation are Tanabe (Wakayama Prefecture) and Kochi (Kochi Prefecture). These locations show large wave heights relative to the local tidal range for earthquake sources down to Mw 8.7. Further, tsunami from Mw 9.0 and larger earthquakes in the Izu–Bonin segment are predicted to be visible at all locations throughout Japan, as well as along the West Coast of the

Americas. It is also notable that Hilo, Hawaii shows consistently large wave heights for magnitudes down to Mw 8.7 as well, particularly in comparison to wave heights at Honolulu, Hawaii (Additional file 3: Figure S2). Thus, given the apparent completeness of records in Wakayama Prefecture back to 1403, we postulate that records of any tsunami from an earthquake greater than Mw 8.7 from an Izu–Bonin source after 1403 should be present in the historic record.

For North Mariana tsunami sources, the most reliable locations for observation are Tanabe (Wakayama Prefecture) and Kuwagasaki (Iwate Prefecture), both of which show a high likelihood of observation down to Mw 8.7. Tsunami from Mw 9.0 and larger earthquakes are predicted to be visible at all locations throughout Japan, as well as at most locations along the West Coast of the Americas. Similar to Izu–Bonin sources, wave heights at Hilo, Hawaii are also consistently large. Given the apparent completeness of records in Wakayama Prefecture and Iwate Prefecture back to 1611, we postulate that any tsunami from an earthquake greater than Mw 8.7 from a North Mariana source possibly after 1403 and certainly after 1611 should have been recorded in the historic record.

For South Mariana tsunami sources, the most reliable locations for observation are Futtsu (Chiba Prefecture) and Otsuchi (Iwate Prefecture) both of which show a high likelihood of observation down to Mw 8.7. Tsunami from Mw 9.0 and larger earthquakes are predicted to be visible at all locations throughout Japan and at low latitude locations along the West Coast of the Americas. Given the apparent completeness of records in Chiba Prefecture and Iwate Prefecture back to 1241, we postulate that any tsunami from an earthquake greater than Mw 8.7 from a South Mariana source possibly after 1241 and certainly after 1611 should have been recorded in the historic record.

For locations in the Americas, our modeling suggests that Lima, Peru, is the most susceptible to large waves from all sources for earthquakes larger than Mw 9.0. Further south, Concepción, Chile appears to be susceptible to large waves from Izu–Bonin sources larger than Mw 9.0 and from Northern and Southern Mariana sources larger than Mw 9.3. Thus, we postulate that any tsunami from an earthquake greater than Mw 9.3 for all sources after 1562 and, for select sources greater than Mw 9.0 after 1586 should have been recorded in the historic record.

Discussion

Candidate IBM earthquakes in the historical record

Interrogating the historical record reveals at least two candidate great subduction zone earthquakes with a source in the IBM: the 1605 Keicho earthquake, and the 1849 Guam earthquake. Considerable attention has been given to the 1605 Keicho earthquake, in part because its effects were experienced along the Nankai region of Japan, a region with numerous great earthquakes in the historical era (Seno 2002; Ishibashi 2004; Ando and Nakamura 2013; Fujino et al. 2018). Out of all of the Nankai Trough earthquakes and tsunami, the 1605 Keicho earthquake is notable for its lack of strong seismic shaking compared with the size of its tsunami spurring interest in whether the 1605 earthquake was a tsunami earthquake (Seno, 2002; Ishibashi, 2004). Following reports of shaking felt in the Kanto and Tohoku districts along with anomalously large tsunami from the 21 December, 2010 Bonin Islands earthquake (Fig. 1)—a shaking and tsunami pattern similar to the 1605 earthquake—Harada et al. (2013) suggested that the 1605 earthquake may have had a source in the Izu–Bonin Islands, rather than the Nankai Trough. Based on the focal mechanism of the 2010 Bonin Islands earthquake, Harada et al. (2013) use a steeply dipping outer-rise fault to model tsunami wave heights to the Nankai region and found good agreement with tsunami reports for the 1605 earthquake. Our modeling of great earthquakes from the Izu–Bonin segment of the IBM is in agreement with that of Harada et al. (2013), showing large tsunami along the south coast of Honshu for sources down to Mw 8.7. Our models suggest that earthquakes larger than Mw 9.0 from the Izu–Bonin segment are expected to be observable throughout Japan, including the northeast coast of Honshu. Since there is no indication that the 1605 tsunami was recorded outside of southern Honshu, it is unlikely to have been as large as Mw 9.0. Finally, although it may be difficult to discriminate between tsunami generated by outer-rise normal faulting earthquake and shallow thrust earthquakes in the historical record, additional records of the 1605 tsunami may shed more light on the source region.

The second candidate great earthquake from the IBM system is the 1849 Guam earthquake. As mentioned previously in the Background Section, the 1849 Guam earthquake destroyed all of the stone structures on the island, created sand boils that discharged sea water, and caused a tsunami that inundated the island in places, up to 402 m (Soloviev and Go 1984a, b; Lander et al. 2002). Both the earthquake and tsunami were also observed on the island of Satawal, over 700 km SSE of Guam, where locals claim to have survived a great earthquake and ensuing flood (Lander et al. 2002). These observations suggest that an ocean-crossing tsunami was generated by this earthquake and should have been observable throughout the Pacific Basin. Our modeling suggests that earthquakes from the South Mariana segment with magnitude larger

Table 2 Water height results for M_w 8.7, M_w 9.0, and M_w 9.3 earthquakes for each fault segment in the Izu–Bonin–Mariana system

Gauge no.	Name	Tidal range (mean range of Tide MN [m])	IB-V Maximum [m]	Percentage	NM-V Maximum [m]	Percentage	SM-V Maximum [m]	Percentage
Magnitude 9.3								
1	Keelung, Taiwan	0.489	2.1	429.45%	0.65	132.92%	1.16	237.22%
2	Toucheng, Taiwan	0.48	3.2	666.67%	0.87	181.25%	− 4.01	835.42%
3	Ginowan, Okinawa	1.2	4.79	399.17%	1.51	125.83%	4.1	341.67%
4	Naha, Okinawa	1.227	2.38	193.97%	1.15	93.72%	2.54	207.01%
5	Tanabe, Japan	0.988	− 6.75	683.20%	2.32	234.82%	3.25	328.95%
6	Kochi, Japan	0.988	5.08	514.17%	1.65	167.00%	2.98	301.62%
7	Miho, Japan	0.8	− 1.93	241.25%	1.1	137.50%	− 3.78	472.50%
8	Otsuchi, Japan	0.711	1.84	258.79%	1.84	258.79%	− 4.19	589.31%
9	Futtsu, Japan	0.802	1.92	239.40%	1.29	160.85%	8.36	1042.39%
10	Kuwagasaki, Japan	0.711	1.85	260.20%	1.63	229.25%	2.69	378.34%
11	Shanghai, China	2.69	0.31	11.52%	0.29	10.78%	0.31	11.52%
12	Hong Kong Island, Hong Kong	0.938	0.78	83.16%	0.45	47.97%	0.45	47.97%
15	Manila, Philippines	0.685	0.17	24.82%	0.11	16.06%	0.15	21.90%
16	Honolulu, United States	0.39	1.27	325.64%	1.61	412.82%	− 0.67	171.79%
17	Hilo, United States	0.51	7.16	1403.92%	− 3.35	656.86%	− 1.65	323.53%
18	Anchorage, United States	7.98		0.00%		0.00%		0.00%
19	Henderson Bay, NZ	2.87	0.89	31.01%	0.41	14.29%	1.33	46.34%
20	Crescent City, United States	1.52	− 5.15	338.82%	− 5.6	368.42%	− 1.08	71.05%
21	Acapulco, Mexico	0.422	− 1.13	267.77%	− 0.73	172.99%	− 0.94	222.75%
22	Ixtapa, Mexico	0.42	− 0.92	219.05%	0.89	211.90%	0.92	219.05%
24	Lima, Peru	0.446	1.03	230.94%	1.66	372.20%	− 1.26	282.51%
25	Concepcion, Chile	0.948	− 2.12	223.63%	− 1.03	108.65%	− 0.57	60.13%
26	Valparaiso, Chile	0.922	− 3.04	329.72%	2.1	227.77%	0.65	70.50%
Magnitude 9.0								
1	Keelung, Taiwan	0.489	1.06	216.77%	− 0.46	94.07%	0.71	145.19%
2	Toucheng, Taiwan	0.48	1.64	341.67%	− 0.55	114.58%	− 3.4	708.33%
3	Ginowan, Okinawa	1.2	1.76	146.67%	1.31	109.17%	2.74	228.33%
4	Naha, Okinawa	1.227	1	81.50%	1.12	91.28%	1.5	122.25%
5	Tanabe, Japan	0.988	− 3.96	400.81%	− 2.75	278.34%	− 2.66	269.23%
6	Kochi, Japan	0.988	3.9	394.74%	− 1.83	185.22%	1.77	179.15%
7	Miho, Japan	0.8	− 1.73	216.25%	0.88	110.00%	− 2.19	273.75%
8	Otsuchi, Japan	0.711	1.15	161.74%	− 2.68	376.93%	− 2.45	344.59%
9	Futtsu, Japan	0.802	2.1	261.85%	0.95	118.45%	5.6	698.25%
10	Kuwagasaki, Japan	0.711	− 1.22	171.59%	1.69	237.69%	1.71	240.51%
11	Shanghai, China	2.69	0.199	7.40%	0.23	8.55%	0.21	7.81%

Table 2 (continued)

Gauge no.	Name	Tidal range (mean range of Tide MN [m])	IB-V Maximum [m]	Percentage	NM-V Maximum [m]	Percentage	SM-V Maximum [m]	Percentage
12	Hong Kong Island, Hong Kong	0.938	0.37	39.45%	0.3	31.98%	0.34	36.25%
15	Manila, Philippines	0.685	0.086	12.55%	0.07	10.22%	0.12	17.52%
16	Honolulu, United States	0.39	0.76	194.87%	0.72	184.62%	0.47	120.51%
17	Hilo, United States	0.51	− 5.2	1019.61%	− 1.99	390.20%	− 1.68	329.41%
18	Anchorage, United States	7.98	0.037	0.46%	− 0.03	0.38%	− 0.04	0.50%
19	Henderson Bay, NZ	2.87	0.56	19.51%	0.31	10.80%	− 0.52	18.12%
20	Crescent City, UnitedStates	1.52	− 3.12	205.26%	− 4.17	274.34%	0.87	57.24%
21	Acapulco, Mexico	0.422	0.644	152.61%	− 0.58	137.44%	− 0.65	154.03%
22	Ixtapa, Mexico	0.42	0.44	104.76%	0.49	116.67%	0.66	157.14%
24	Lima, Peru	0.446	0.59	132.29%	0.73	163.68%	− 0.82	183.86%
25	Concepcion, Chile	0.948	− 1.13	119.20%	− 0.71	74.89%	− 0.34	35.86%
26	Valparaiso, Chile	0.922	− 1.57	170.28%	− 1.15	124.73%	0.41	44.47%
Magnitude 8.7								
1	Keelung, Taiwan	0.489	0.42	85.89%	− 0.22	44.99%	0.24	49.08%
2	Toucheng, Taiwan	0.48	0.64	133.33%	− 0.25	52.08%	− 0.72	150.00%
3	Ginowan, Okinawa	1.2	0.8	66.67%	0.62	51.67%	0.92	76.67%
4	Naha, Okinawa	1.227	− 0.45	36.67%	0.46	37.49%	− 0.74	60.31%
5	Tanabe, Japan	0.988	− 1.42	143.72%	− 1.13	114.37%	− 0.8	80.97%
6	Kochi, Japan	0.988	1.49	150.81%	− 0.76	76.92%	0.63	63.77%
7	Miho, Japan	0.8	− 0.57	71.25%	0.36	45.00%	− 0.74	92.50%
8	Otsuchi, Japan	0.711	0.43	60.48%	− 1.07	150.49%	− 0.833	117.16%
9	Futtsu, Japan	0.802	0.73	91.02%	0.46	57.36%	2.15	268.08%
10	Kuwagasaki, Japan	0.711	− 0.48	67.51%	− 0.92	129.40%	0.58	81.58%
11	Shanghai, China	2.69	0.11	4.09%	0.13	4.83%	0.1	3.72%
12	Hong Kong Island, Hong Kong	0.938	0.12	12.79%	0.1	10.66%	− 0.09	9.59%
15	Manila, Philippines	0.685	0.04	5.84%	0.03	4.38%	0.04	5.84%
16	Honolulu, United States	0.39	0.29	74.36%	0.31	79.49%	0.17	43.59%
17	Hilo, United States	0.51	− 2.3	450.98%	− 0.98	192.16%	− 0.5	98.04%
18	Anchorage, United States	7.98		0.00%		0.00%		0.00%
19	Henderson Bay, NZ	2.87	− 0.02	0.70%	0.02	0.70%	0.12	4.18%
20	Crescent City, United States	1.52	− 1.05	69.08%	− 1.86	122.37%	0.07	4.61%
21	Acapulco, Mexico	0.422	0.24	56.87%	− 0.28	66.35%	− 0.23	54.50%
22	Ixtapa, Mexico	0.42	0.18	42.86%	0.24	57.14%	0.22	52.38%

Table 2 (continued)

Gauge no.	Name	Tidal range (mean range of Tide MN [m])	IB-V Maximum [m]	Percentage	NM-V Maximum [m]	Percentage	SM-V Maximum [m]	Percentage
24	Lima, Peru	0.446	−0.16	35.87%	−0.25	56.05%	0.02	4.48%
25	Concepcion, Chile	0.948	−0.4	42.19%	−0.3	31.65%	0.03	3.16%
26	Valparaiso, Chile	0.922	−0.53	57.48%	0.47	50.98%	−0.06	6.51%

Water heights are shown as a percentage of the local mean range of tides as determined from nearby sea level monitoring stations from the GLOSS network (see Table 1)

than Mw 9.0 should be visible at all locations in Japan; Honolulu and Hilo, Hawaii; and low latitude sites along the west coast of the Americas. Observability decreases for earthquakes in the South Mariana fault segment with magnitudes of Mw 8.7, but most locations remain in the *Possibly Observable* category. Given the apparent lack of tsunami reports from Japan for the 1849 Guam earthquake and tsunami, the magnitude of the 1849 Guam earthquake must have been less than Mw 8.7.

Sensitive locations

Some locations seem especially sensitive to IBM earthquakes with magnitudes as low as Mw 8.7 producing wave heights in the *Likely Observable* category. For example, modeling predicts wave heights in Hilo, Hi of 7.16 m from an Mw 9.3 Izu–Bonin earthquake, at an astonishing 1400% of the local tidal range (Table 2). Other locations, such as Toucheng, Taiwan, on the northeast coast of Taiwan could experience wave heights of 4 m for Mw 9.3 Izu–Bonin sources (835% of the tidal range). The wave heights in Toucheng, Taiwan, stand in contrast to those of nearby Keelung, Taiwan, a major port which appears to gain some protection from IBM tsunami by virtue of its location in the lee of the Yilan peninsula (Additional file 3: Figure S2). Both the wave heights at Hilo and the Toucheng appear to be due to focusing of wave energy by undersea bathymetry. This effect has been noted by others at Hilo, Hawaii (e.g., Tang et al. 2010).

Other locations, such as Tanabe, Japan are predicted to experience *Likely Observable* wave heights for all faulting scenarios at all magnitude except South Mariana sources with magnitudes of Mw 8.7. Otsuchi, Japan, is similar in that it is expected to experience *Likely Observable* wave heights for all sources and magnitude except Izu–Bonin sources with magnitudes of Mw 8.7. In both locations, the largest wave arrival varies between scenarios suggesting a complex interplay of bathymetric, wave reflection, and resonance effects (Additional file 4: Figure S3). The consistency of these observations suggests that paleoseismic studies in these areas should consider IBM sources.

Other measures of observability

Our approach to estimating tsunami observability focuses heavily on comparing the predicted tsunami wave heights to the local tidal range. However, coastal residents can be in tune to other changes to the ocean that would also indicate the arrival of a tsunami.

For example, many tsunami reports in the NCEI/WDS database note changes in the speed and direction of the currents within harbors. Tsunami modeling software, such as GeoClaw, can calculate the horizontal flow velocity, and future research could explore the interplay between tsunami observability and horizontal flow velocity at low wave-height locations.

Another factor influencing the eyewitness observation of tsunami is the time of arrival. For tsunami arriving at night, the first (and often largest) waves can be missed. This appears to be the case with the tsunami from the 1906 Ecuador earthquake, which was observed in Gisborne approximately 8–10 h later than expected leading some to suggest that the initial, and largest, waves arrived during the night and went unnoticed (GNS Science 2020). Similarly, the combination of a nighttime arrival and an arrival during low tide for the first waves from the tsunami generated by the 1868 Peru earthquake as observed at various locations throughout the South Island of New Zealand led to poor observation of the wave heights and arrival times there (GNS Science 2020).

The ability to observe tsunami can also be greatly affected by how calm the sea is during the arrival of the waves. For example, the 28 Feb 1973 Kuril Island tsunami produced only fragmentary eyewitness reports of tsunami run-up mostly due to stormy weather in the region (National Geophysical Data Center 2022). In the historical record, stormy seas can both hinder observation of tsunami and create the false impression of a tsunami (e.g., a meteotsunami).

Conclusions

We have modeled tsunami from megathrust sources in the Izu–Bonin and Mariana subduction zone and calculated maximum wave heights for select locations

around the Pacific Basin with a focus on those with long written histories of tsunami observations. For an earthquake larger than Mw 9.0, the resulting tsunami would be visible at a large number of locations in the Pacific Basin. Assuming the completeness of written records of tsunami at our chosen locations, this would constrain the magnitude of the largest earthquake from the Izu–Bonin–Mariana system to less than Mw 8.7 since at least 1605. For earthquakes smaller than Mw 8.7 few far-field locations in the Pacific Basin would be expected to receive maximum wave heights sufficient to be observable without marigrams. Future research into written historical records of tsunami inundation around the Pacific Basin should therefore consider IBM tsunami sources with Mw > 9.0.

Supplementary Information

The online version contains supplementary material available at https://doi.org/10.1186/s40623-022-01748-6.

Additional file 1: Table S1. Model earthquake fault definitions. Earthquakes were defined as slip on faults from the NOAA SIFT model (Gica et al. 2008). Faults from this model are divided into SIFT subduction zones (i.e., KISZ for the Kamchatka–Yap–Mariana-Izu–Bonin system) and sub-fault letter identifiers (i.e., a1, b1, a2, etc.). Column "Model Tsunami Source" lists the amount of slip on each sub-fault. Fault latitude, longitude, strike, dip, depth and fault area for each sub-fault are defined in Gica et al. 2008.

Additional file 2: Figure S1. Slip distributions of each of model earthquake scenarios used in this study. Slip amounts and fault definitions are listed in Table S1. Color scale in Figure e applies to all slip distributions and shows fault slip in meters. Figures a, b, and c, show scenario earthquakes in the Izu–Bonin segment of the IBM with magnitudes M_w 8.7, M_w 9.0, and M_w 9.3, respectively. Figures d, e, and f, show scenario earthquakes in the Northern Mariana segment of the IBM with magnitudes M_w 8.7, M_w 9.0, and M_w 9.3, respectively. Figures g, h, and i, show scenario earthquakes in the Southern Mariana segment of the IBM with magnitudes M_w 8.7, M_w 9.0, and M_w 9.3, respectively.

Additional file 3: Figure S2. Example tsunami waveforms from the South Mariana M_w 9.3 and Izu–Bonin M_w 8.7 earthquake scenarios highlighting differences in wave heights between nearby gauges. Wave heights in a., show how the Yilan peninsula of Taiwan appears to act as a barrier to wave energy from the southeast resulting in reduced wave heights appearing in Keelung as compared with Toucheng for a tsunami source in the South Mariana with magnitude M_w 9.3. Figure b. shows the difference between wave heights predicted for Honolulu and Hilo, Hawaii reflecting bathymetric and directivity effects from Izu–Bonin M_w 8.7 sources. Great circle paths from the Izu–Bonin trench to Honolulu, Hawaii are blocked by the island of Oahu resulting in reduced wave heights whereas those to Hilo are relatively unobstructed.

Additional file 4: Figure S3. Tsunami waveforms for M_w 9.0 sources in the Izu–Bonin, North Mariana, and South Mariana subduction zone at (a.) Otsuchi and (b.) Tanabe, Japan. Note how the largest amplitude waves occur at different points in the wave train for each source, suggesting that differing path effects, wave reflections, and local resonances each play a role in maintaining the high wave amplitudes in each scenario.

Additional file 5: Figure S4. Example waveforms comparing the effects of dispersion on tsunami from the M_w 9.0 source in the South Mariana subduction zone at (a.) Kochi, (b.) Tanabe, and (c.) Miho, Japan. All three locations are approximately 2600 km away from the tsunami source and show only minor changes to higher frequency components of the waveforms as predicted using Eq. (1) in Shuto (1991). Both waveforms with and without dispersion were calculated with JAGURS (Baba et al. 2015).

Acknowledgements
We would like to acknowledge K. Satake for pointing us towards prior tsunami modeling from the Izu–Bonin trench. We would also like to acknowledge Brian Atwater for discussions regarding Japanese tsunami record sources. Additionally, we would like to thank Stacey Martin and an anonymous reviewer for helpful feedback that greatly improved this manuscript.

Author contributions
WS composed the manuscript, refined the tsunami models, and created the figures. RR performed modeling of sources and initial assessment of results. BM provided material assistance in model set-up and assessment of tsunami models. Both RR and BM assisted in editing the manuscript for publication. All authors read and approved the final manuscript.

Funding
Funding for the preparation of this manuscript was provided by Central Washington University.

Availability of data and materials
NOAA Sift Model Location: https://sift.pmel.noaa.gov/, Global Bathymetry: https://www.gebco.net/, GLOSS Data: https://uhslc.soest.hawaii.edu/gloss/, National Geophysical Data Center / World Data Service: NCEI/WDS Global Historical Tsunami Database. NOAA National Centers for Environmental Information. https://doi.org/10.7289/V5PN93H7, Jan 2022. GNS Science. (2020). New Zealand Tsunami Database: Historical and Modern Records [Data set]. GNS Science. https://doi.org/10.21420/D6W9-0G74s. Tidal ranges for some locations were estimated using OTPS (Egbert and Erofeeva 2002). Tsunami run-ups for the Dec 21, 2010 Bonin Island tsunami are from the National Tsunami Warning Center, Recent Tsunamis, https://tsunami.gov/recent_tsunamis/ Accessed Feb 2022. Source code for GeoClaw is available from http://www.clawpack.org. Source code for JAGURS is available from https://github.com/jagurs-admin/jagurs. Instrumental earthquake locations courtesy of the US Geological Survey's Advanced National Seismic System (ANSS) Comprehensive Catalog of Earthquake Events and Products. https://doi.org/10.5066/F7MS3QZH.

Declarations

Competing interests
The authors declare no competing interests.

Author details
[1]Central Washington University, Ellensburg, WA, USA. [2]University of Texas, El Paso, TX, USA.

Received: 14 June 2022 Accepted: 7 December 2022
Published online: 30 December 2022

References

Ambraseys N, Melville CP (1982) A History of Persian Earthquakes. 219p. Cambridge Univ. Press, Cambridge

Ando M, Nakamura M (2013) Seismological evidence for a tsunami earthquake recorded four centuries ago on historical documents. Geophys J Int 195:1088–1101. https://doi.org/10.1093/gji/ggt270

Baba T, Takahashi N, Kaneda Y, Ando K, Matsuoka D, Kato T (2015) Parallel implementation of dispersive tsunami wave modeling with a nesting algorithm for the 2011 Tohoku tsunami. Pure Appl Geophys 172:3455–3472. https://doi.org/10.1007/s00024-015-1049-2

Baba T, Allgeyer S, Hossen J, Cummins PR, Tsushima H, Imai K, Yamashita K, Kato T (2017) Accurate numerical simulation of the far-field tsunami caused by the 2011 Tohoku earthquake, including the effects of Boussinesq dispersion, seawater density stratification, elastic loading, and gravitational potential change. Ocean Model 111:46–54. https://doi.org/10.1016/j.ocemod.2017.01.002

Barnes PM, Nicol A, Harrison T (2002) Late Cenozoic evolution and earthquake potential of an active listric thrust complex above the Hikurangi subduction zone, New Zealand. GSA Bull 114:1379–1405. https://doi.org/10.1130/0016-7606(2002)114%3c1379:LCEAEP%3e2.0.CO;2
Ben-Menahem A, Rosenman M (1972) Amplitude patterns of tsunami waves from submarine earthquakes. J Geophys Res 77(17):3097–3128
Beringhausen WH (1962) Tsunamis reported from the west coast of South America 1562–1960. Bull Seismo Soc Am 52(4):915–921
Caldwell PC, Merrifield MA, Thompson (2015) Sea level measured by tide gauges from global oceans—the Joint Archive for Sea Level holdings (NCEI Accession 0019568), Version 5.5, *NOAA National Centers for Environmental Information*, Dataset, https://doi.org/10.7289/V5V40S7W
Campos J, Madariaga R, Scholz C (1996) Faulting Process of the August 8, 1993, Guam earthquake: a thrust event in an otherwise weakly coupled subduction zone. J Geophys Res 101(B8):17581–17596
Cholmondeley LB (1915) The history of the Bonin Islands from the year 1827 to the year 1876 and of Nathaniel Savory, one of the original settlers, to which is added a short supplement dealing with the islands after their occupation by the Japanese. Archibald Constable, London
Clawpack Development Team (2020), Clawpack Version 5.7.1, http://www.clawpack.org, doi: 10.5281/zenodo.4025432
Cox DC (1872) Lander JF (1994) Revised Source of the Tsunami of August 23. Sci Tsunami Hazards 12(2):117–126
Davis BN, LeVeque RJ (2016) Adjoint methods for guiding adaptive mesh refinement in tsunami modeling. Pure Appl Geophys 173:4055–4074. https://doi.org/10.1007/978-3-319-55480-8_19
De Lange WP, Healy TR (1986) New Zealand tsunamis 1840–1982. N Z J Geol Geophys 29(1):115–134. https://doi.org/10.1080/00288306.1986.10427527
Egbert GD, Erofeeva SY (2002) Efficient inverse modeling of barotropic ocean tides. J Atmos Ocean Tech 19(2):183–204. https://doi.org/10.1175/1520-0426(2002)019%3c0183:EIMOBO%3e2.0.CO;2
Fujino S, Kimura H, Komatsubara J, Matsumoto D, Namegaya Y, Sawai Y, Shishikura M (2018) Stratigraphic evidence of historical and prehistoric tsunamis on the Pacific coast of central Japan: Implications for the variable recurrence of tsunamis in the Nankai Trough. Quat Sci Rev 201:147–161. https://doi.org/10.1016/j.quascirev.2018.09.026
GEBCO Compilation Group (2019) GEBCO 2019 Grid. https://doi.org/10.5285/836f016a-33be-6ddc-e053-6c86abc0788e
Gica E, Spillane MC, Titov VV, Chamberlin CD, Newman JC (2008) Development of the forecast propagation database for NOAA's Short-term Inundation Forecast for Tsunamis (SIFT): NOAA Tech. Memo. OAR PMEL-139, p. 89, http://www.ntis.gov (accessed May 2020)
Gill SK, Schultz JR (eds) (2001) Tidal datums and their applications. Silver Spring MD, NOAA, NOS Center for Operational Oceanographic Products and Services, 102pp. & Appendix. (NOAA Special Publication NOS CO-OPS 1). https://doi.org/10.25607/OBP-170
Goldfinger C, Kulm LD, Yeats RS, Appelgate B, MacKay ME, Moore GF (1992) Transverse structural trends along the Oregon convergent margin: Implications for Cascadia earthquake potential and crustal rotations. Geology 20:141–144. https://doi.org/10.1130/0091-7613(1992)020%3c0141:TSTATO%3e2.3.CO;2
Harada T, Ishibashi K (2008) Interpretation of the 1993, 2001, and 2002 Guam Earthquakes as Intraslab Events by a Simultaneous Relocation of the Mainshocks, Aftershocks, and Background Earthquakes. Bull Seismo Soc Am 98(3):1581–1587. https://doi.org/10.1785/0120060227
Harada T, Ishibashi K, Satake K (2013) Tsunami Numerical Simulation for Hypothetical Giant or Great Earthquakes along the Izu-Bonin Trench. American Geophysical Union, In AGU Fall Meeting Abstracts
Heaton TH, Kanamori H (1984) Seismic potential associated with subduction in the northwestern United States. Bull Seismol Soc Am 74(3):933–941
Ishibashi K (2004) Status of historical seismology in Japan. Ann Geophys 47(2/3):339–368. https://doi.org/10.4401/ag-3305
Johnson JM, Satake K (1999) Asperity Distribution of the 1952 Great Kamchatka Earthquake and its Relation to Future Earthquake Potential in Kamchatka. Pure Appl Geophys 154:541–553. https://doi.org/10.1007/978-3-0348-8679-6_8
Kagan YY, Jackson DD (2013) Tohoku earthquake: a surprise? Bull Seismol Soc Am 103(2B):1181–1194. https://doi.org/10.1785/0120120110
Kanamori H (1986) Rupture process of subduction-zone earthquakes. Ann Rev Earth Planet Sci 14:293–322
Lander JF, Whiteside LS, Hattori P (2002) The Tsunami History of Guam: 1849–1993. Sci Tsunami Haz 20(3):158–174
Lander JF, Lockridge PA (1989) United States Tsunamis (including United States Possessions): 1690–1988. Publication 41–2, National Geophysical Data Center, Boulder, CO
Lander JF, Lockridge PA, Kozuch MJ (1993) Tsunamis affecting the West Coast of the United States, 1806–1992. NGDC Key to Geophysical Records Documentation No. 29. US Department of Commerce, Boulder, CO
Lau AYA, Switzer AD, Dominey-Howes D, Aitchison JC, Zong Y (2010) Written records of historical tsunamis in the northeastern South China Sea—challenges associated with developing a new integrated database. Nat Haz Earth Sys Sci 10:1793–1806. https://doi.org/10.5194/nhess-10-1793-2010
Liu Y, Santos A, Wang SM, Shi Y, Liu H, Yuen DA (2007) Tsunami hazards along Chinese coast from potential earthquakes in South China Sea. Phys Earth Planet Int 163:233–244. https://doi.org/10.1016/j.pepi.2007.02.012
Lockridge PA (1985) Tsunamis in Peru-Chile. Report SE-39, National Geophysical Data Center, Boulder, CO
Ludwin RS, Smits GJ, Carver D, James K, Jonientz-Trisler C, McMillan AD, Losey R, Dennis R, Rasmussen J, De Los Angeles A, Buerge D, Thrush CP, Clague J, Bowechop J, Wray J (2007) Folklore and earthquakes: Native American oral traditions from Cascadia compared with written traditions from Japan. from Piccardi L, Masse WB (eds) Myth and Geology. Geological Society, London. Special Publications, 273:67–94
Lutton N (1991) Archives and national identity in Papua New Guinea. Arch Manu 19(2):181–191
Martin SS, Wang Y, Muzli M, Wei S (2020) The 1922 Peninsular Malaysia earthquakes: rare intraplate seismicity within the sundaland block in southeast Asia. Seism Res Lett 91(5):2531–2545. https://doi.org/10.1785/0220200052
Matsu'ura RS (2017) A short history of Japanese historical seismology: past and present. Geosci Lett 4:3. https://doi.org/10.1186/s40562-017-0069-4
McCaffrey R (2008) Global frequency of magnitude 9 earthquakes. Geology 36(3):263–266. https://doi.org/10.1130/G24402A.1
Nagle P (2002) Papua New Guinea records 1883–1942: Microfilm collections. Research Guide 4, National Archives of Australia. https://www.naa.gov.au/sites/default/files/2020-06/research-guide-papua-new-guinea-records.pdf
National Geophysical Data Center / World Data Service: NCEI/WDS Global Historical Tsunami Database. NOAA National Centers for Environmental Information. doi:https://doi.org/10.7289/V5PN93H7, Jan 2022
National Tsunami Warning Center, Recent Tsunamis, https://tsunami.gov/recent_tsunamis/. Accessed Feb 2022
O'Loughlin KF, Lander JF (2003) Caribbean Tsunamis: A 500 year history from 1498–1998. 263p. Dordrecht, Boston
Pararas-Carayannis G (1977) Catalog of Tsunamis in Hawaii. Revised 1977, Report SE-4, World Data Center A for Solid Earth Geophysics, US Dept Commerce, Boulder, CO
Punlazan RL (2006) Archives of the new possession: Spanish colonial records and the American creation of a "national" archives for the Philippines. Arch Sci 6:381–392. https://doi.org/10.1007/s10502-007-9040-z
Rong Y, Jackson DD, Magistrale H, Goldfinger C (2014) Magnitude limits of subduction zone earthquakes. Bull Seismol Soc Am 104(5):2359–2377. https://doi.org/10.1785/0120130287
Ruff LJ (1989) Do trench sediments affect great earthquake occurrences in subduction zones? Pure Appl Geophys 129(1/2):263–282
Ruff L, Kanamori H (1980) Seismicity and the subduction process. Phys Earth Planet in 23(3):240–252
Sanchez AJ, Farreras SF (1993) Catalog of tsunamis on the western coast of Mexico. Report SE-50, World Data Center A for Solid Earth Geophysics, NOAA, National Geophysical Data Center, Boulder, Colorado, USA, 79 p
Satake K, Atwater BF (2007) Long-term perspectives on giant earthquakes and tsunamis at subduction zones. Ann Rev Earth Planet Sci 35:349–374. https://doi.org/10.1146/annurev.earth.35.031306.140302
Satake K, Kanamori H (1991) Abnormal Tsunamis Caused by the June 13, 1984, Torishima, Japan. Earthquake J Geophys Res 96(B12):19933–19939
Satake K, Shimazaki K, Tsuji Y, Ueda K (1996) Time and size of a giant earthquake in Cascadia inferred from Japanese tsunami records of January 1700. Nature 379(6562):246–249

GNS Science (2020) New Zealand Tsunami Database: Historical and Modern Records . GNS Science. https://doi.org/10.21420/D6W9-0G74
Seno T (2002) Tsunami earthquakes as transient phenomena. Geophys Res Lett 29:10. https://doi.org/10.1029/2002GL014868
Shuto N (1991) Numerical Simulation of Tsunamis—Its Present and Near Future. Nat Haz 4:171–191
Sigrist DJ (1995) Tsunamis in Guam Tsunami Newsletter 27:20
Singh SK, Astiz L, Havskov J (1981) Seismic gaps and recurrence periods of large earthquakes along the Mexican subduction zone: a reexamination. Bull Seismo Soc Am 71:827–843
Soloviev SL, Go CN (1984a) A catalogue of tsunamis on the western shore of the Pacific Ocean (173–1968). volume 5077 of Can. Transl. Fish. Aquat. Sci., page 310. Nauka Publishing House, Moscow, USSR
Soloviev SL, Go CN (1984b) A catalogue of tsunamis on the eastern shore of the Pacific Ocean (1513–1968). volume 5078 of Can. Transl. Fish. Aquat. Sci., page 310. Nauka Publishing House, Moscow, USSR
Stein S, Okal E (2011) The size of the 2011 Tohoku earthquake need not have been a surprise. Eos Trans Am Geophys Union 92(27):227–228. https://doi.org/10.1029/2011EO270005
Stern RJ (2002) Subduction zones. Rev Geophys 40:4. https://doi.org/10.1029/2001RG000108
Stern RJ, Fouch MJ, Klemperer SL (2003) An Overview of the Izu-Bonin-Mariana subduction factory. in inside the subduction factory. Elier J (ed) 138:175–222. https://doi.org/10.1029/138GM10
Tang L, Titov VV, Chamberlin CD (2010) A Tsunami Forecast Model for Hilo, Hawaii. NOAA OAR Special Report, PMEL Tsunami Forecast Series: Vol 1. US Dept. Commerce. 96 p
Tanioka Y, Satake K, Ruff L (1995) Analysis of Seismological and Tsunami Data from the 1993 Guam Earthquake. Pure Appl Geophys 144(3/4):823–837
US Geological Survey, Earthquake Hazards Program, (2017), Advanced National Seismic System (ANSS) Comprehensive Catalog of Earthquake Events and Products: Various. Accessed June 2019. https://doi.org/10.5066/F7MS3QZH
Uyeda S, Kanamori H (1979) Back-arc opening and the mode of subduction. J Geophys Res 84(B3):1049–1061
Zhao X, Jiang Y, Ren Z, Liu H (2017) Historical tsunami records and potential tsunami scenarios near Haikou coastal region. Nat Hazards 89:625–645. https://doi.org/10.1007/s11069-017-2983-3

Publisher's Note